Dielectronic recombination measurements of P^{4+}, S^{5+}, and Cl^{6+}

P. F. Dittner, S. Datz, P. D. Miller, and P. L. Pepmiller
Oak Ridge National Laboratory, Oak Ridge, Tennessee 37831

C. M. Fou
Department of Physics, University of Delaware, Newark, Delaware 19711
(Received 15 July 1985)

Dielectronic recombination via $3s$-$3p$ excitation has been measured for the Na-like ions P^{4+}, S^{5+}, and Cl^{6+}. We observed the amount of electron capture attending the passage of MeV/amu ion beams through a collinear, magnetically confined space-charge-limited electron beam as a function of relative energy. The measured rates fall between limits calculated from limiting-case theoretically predicted cross sections.

I. INTRODUCTION

Much current interest in the area of atomic collision physics centers on interactions of multiply charged ions with atoms, ions, and electrons. Aside from strong intrinsic interest in this field, knowledge obtained from such work has application in modeling high-temperature plasmas such as those found in stellar coronae and controlled fusion devices.

Electron-ion collisions can lead to ionization, excitation, or recombination. Here we center on recombination, in particular, dielectronic recombination (DR) in which a continuum electron excites a previously bound electron and is captured into an autoionizing state. The resulting doubly excited ion of the next lower charge state may either emit a photon resulting in DR or it may autoionize. Thus for an ion A of charge q in initial state α, the simplest DR process may be written

$$A^{q+}(\alpha)+e \rightleftarrows [A^{(q-1)+}(\beta;n,l)]^{**} \rightarrow [A^{(q-1)+}(\alpha;n,l)]^{*}+h\nu_{\beta\alpha}\ , \quad (1)$$

where β describes the core excited state of $A^{(q-1)+}$, n and l are the principal and angular momentum quantum numbers of the captured electron, and $\nu_{\beta\alpha}$ is the frequency of the emitted radiation of the core relaxation $\beta \rightarrow \alpha$.

Until 1983 the only experimental information on DR had come from spectroscopic observations of plasmas,[1] from which only thermally averaged rates may be inferred. In 1983–1984 four groups reported DR cross-section measurements. A group at the Joint Institute for Laboratory Astrophysics[2] (JILA) measured the DR cross section for Mg^{+} using crossed ion-electron beams and recording coincidences between recombined Mg atoms and stabilizing photons from the collision region. A similar experiment was carried out by Williams[3] for Ca^{+}. Using merged-electron-ion-beam methods, a group[4] at the University of Western Ontario investigated C^{+} and our group[5] at Oak Ridge National Laboratory (ORNL) studied the Li-like ions B^{2+} and C^{3+}.

In this paper we report on our measurements of DR for the Na-like ions P^{4+}, S^{5+}, and Cl^{6+}. The DR process measured for these ions is

$$A^{q+}(\text{Ne core}, 3s)+e \rightleftarrows A^{(q-1)+}(\text{Ne core}, 3p;n,l) \rightarrow A^{(q-1)+}(\text{Ne core}, 3s;n,l)+h\nu_{3p3s}\ , \quad (2)$$

where the symbols are as described for Eq. (1) and Ne core stands for a $1s^2 2s^2 2p^6$ configuration of electrons. We shall describe the experimental apparatus, experimental procedure, data reduction, and a comparison with theory.

II. EXPERIMENTAL APPARATUS

We chose a merged-beam approach to take advantage of our ability to produce a high-charge state of MeV/amu ions, and a high-current, high-energy electron beam. The merged-beam apparatus (outlined in Fig. 1) is constructed such that in the interaction region the ion beam is coaxial with and embedded within the electron beam for a distance of 84 cm.

The ion beam from the ORNL EN-tandem accelerator enters the interaction region through an axial, 0.64-mm-diam hole in the cathode of the electron gun. After exiting the interaction region, the ion beam is charge-state-analyzed using an electrostatic deflector. The length and separation of the plates is 25 and 1 cm, respectively, and from -3 to -6 kV was applied to the top plate while the bottom plate was grounded. Ions with the initial charge state $q+$ are deflected into a Faraday cup having electrostatic secondary-electron suppression. The cup is connected to a current integrator and the output pulses are counted by a scalar. Ions that have picked up an electron

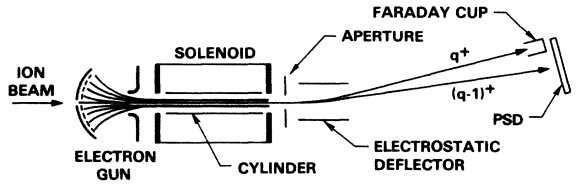

FIG. 1. Schematic diagram of the apparatus.

[charge of $(q-1)+$] are deflected onto a solid-state position-sensitive detector (PSD). The ions having charge $(q-1)+$ arise from electron pickup by the $q+$ ions from the residual-gas molecules, slit-edge scattering, and the sought after effect, DR.

The source of the electron beam is a doubly gridded Pierce-type high-intensity electron gun[6] which is designed to produce a convergent, laminar electron beam. The gun was operated in the space-charge-limited mode where the space-charge-limited current I_c is given in terms of the cathode-to-anode voltage V_c by $I_c = PV_c^{3/2}$. The constant P (the "perveance") is determined by the electrode geometry and grid voltage and equals 10^{-6} here. The electron gun is magnetically shielded from the solenoidal field of the interaction region. The emerging electron beam comes to a focus ~ 7 mm from the anode, where it has a diameter (containing 95% of the beam) of 3.15 mm. It enters a coaxial solenoidal magnetic field which is adjusted to establish Brillouin flow[7] (e.g., ~ 0.018 T for 1-keV electrons) in which the beam radius stays constant and the beam rotates as a solid of revolution about its axis with the Larmor frequency ω_L. Under Brillouin flow the longitudinal velocity of an electron is independent of radius, the radial velocity is zero, and the azimuthal velocity is equal to ω_L times the radial position of that electron. Surrounding the electron beam is a coaxial stainless-steel cylinder (length 84 cm, id 7.9 mm) to which an electrical bias can be applied. The cylinder serves both to minimize the potential difference between the center of the electron beam and ground and, with the application of a voltage, to change the electron velocity at fixed V_c. Following the interaction region, defined by the length of the coaxial cylinder and the solenoidal field, the electron beam expands due to space-charge repulsion and strike the chamber walls.

The entire system is bakable to ~ 200 °C and pressures of 8×10^{-10}–2×10^{-9} Torr are achieved using three 270-l/s combination sublimator-ion pumps and two cryopumps. Operation of the electron gun increases the pressure at the gun and where the electron beam is "dumped." The pressure in the gun region returns to base values ($\sim 1\times10^{-9}$ Torr) after a few hours, but the pressure in the "dump" chamber remains above base values throughout the experiment. The pressure rise in the "dump" region is from 5×10^{-9} to 2×10^{-8} Torr and depends on the voltage and/or current of the electron beam.

III. EXPERIMENTAL PROCEDURE

By considering Eq. (2) one can see that the relative energy (E_r) region in which DR can occur must be such that $0 \le E_r \le E_m$, where E_m is equal to the energy difference between the $3p$ and $3s$ levels in the A^{q+} ion, 11.0, 13.2, and 15.4 eV for P^{4+}, S^{5+}, and Cl^{6+}, respectively. The relative or center-of-mass energy of an ion and a collinear electron is given by

$$E_r = \mu[E_e/m_e + E_i/M_i - 2(E_eE_i/m_eM_i)^{1/2}] , \quad (3)$$

where μ is the reduced mass ($\approx m_e$), E_e and m_e are the energy and mass of the electron, and E_i and M_i are the energy and mass of the ion, respectively. In our experimental arrangement collinearity can only be achieved on the ion- (or electron-) beam axis due to the angular velocity of the electrons about the axis. Radial and angular misalignments of the two beams, angular divergence of the ion beam, and non-Brillouin-flow electron-beam behavior further invalidate Eq. (3). However, these effects primarily produce a spread in E_r (see discussion below on the signal shape) and we will use Eq. (3) to give the centroid E_r. The electron energy to be used in Eq. (3) is not equal to eV_c, but to $\sim 0.96eV_c$, due to the space-charge potential drop of the electron beam from its center to the surrounding tube.[8]

The relative energy can be varied by changing V_c, keeping E_i fixed at the maximum energy E_{im} available from the EN tandem [$E_{im} \approx 6\times(q+1)$ MeV] or fixing $V_c \approx (6\times10^3)(q+1)m_e/M_i$ kV and changing E_i. The choice is dictated by which procedure gives the better signal-to-background ratio. By "background" we mean that part of the $(q-1)+$ ion fraction due to electron pickup by $q+$ ions from the residual gas (RG) and slit edges (SE's). We can define a background ratio R_b as

$$R_b = I_b^{(q-1)+}/I^{q+} = \alpha PE_i^{-n} + \beta E_i^{-m} , \quad (4)$$

where the first term on the right-hand side is due to RG and the second SE, $I_b^{(q-1)+}$ and I^{q+} are the numbers of $(q-1)+$ and $q+$ ions per second, respectively, α is a constant determined by $q+$ and the composition of RG, β is a constant determined by $q+$ and the geometry and composition of SE, P is the RG pressure, and n and m (constants over our range of E_i) are determined by factors listed for α and β. We also find that $2 < n \approx m < 4$. With fixed $E_i = E_{im}$, R_b is minimized, but changing V_c changes P in a nonlinear and not always reproducible manner, and thus R_b cannot easily be determined. Modulation of the electron beam, via square-wave modulation of the control grid bias, produced pressure modulation and thus R_b modulation equal to or greater than expected signals.

We chose to fix V_c at a value determined by E_{im} with $E_r = 0$. This maximizes the electron-beam density ρ_e and minimizes R_b, although R_b will vary as E_i is changed. After setting the grid voltage to obtain a perveance of 1×10^{-6}, we optimized the electron beam by adjusting the orientation of the solenoid and the cylinder surrounding the electron beam (see Fig. 1) and making small adjustments to the solenoidal field such that the current to the cylinder was a minimum ($< 0.01I_c$). It was then verified, by observing the position spectrum of the $(q-1)+$ ions while switching the electron beam on and off, that the electrostatic field, due to the electron space charge, produced no steering of the ion beam. We believe that minimum ion-beam steering indicates minimum misalignment between the ion- and electron-beam axes. An 11-Hz square-wave voltage V_t, alternating between 0 and $+V_t$ (referenced to ground), was applied to the surrounding cylinder. V_t is chosen such that the electron energy [$E_e \sim e(-V_c + V_t)$] together with E_i result in an E_r at least 5 eV above E_m, i.e., a region where no DR signal is expected. We count the $A^{(q-1)+}$ and A^{q+} beams taking ~ 1-eV steps in E_r by changing E_i. The number of ions when V_y is zero, $A_0^{(q-1)+}$ and A_0^{q+}, or V_t, $A_v^{(q-1)+}$ and

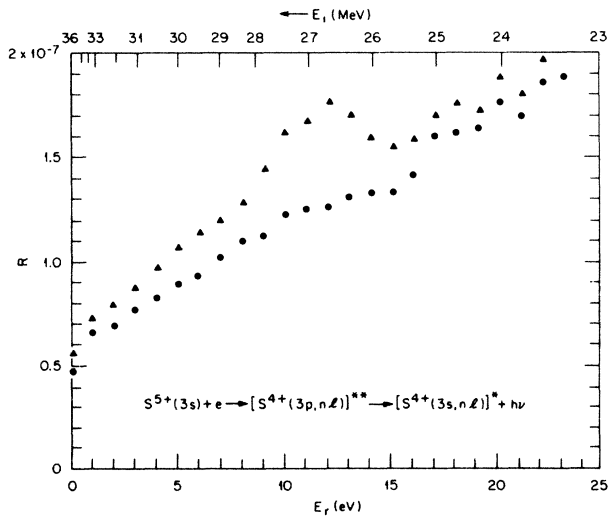

FIG. 2. Ratios R_0 (▲) and R_v (●) vs E_r (lower scale) and E_i (upper scale) for S^{5+}. See text for the definition of R_0 and R_v.

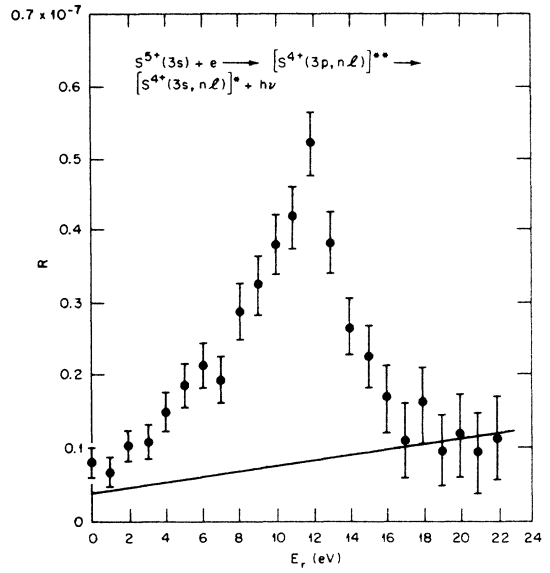

FIG. 3. Difference R $(=R_0-R_v)$ vs E_r for S^{5+}. The solid line is a plot of KE_i^{-n}.

A_v^{q+} are stored in separate channels. At each E_i, we take the ratios

$$R_0(E_i)=A_0^{(q-1)+}(E_i)/A_0^{q+}(E_i)$$

and

$$R_v(E_i)=A_v^{(q-1)+}(E_i)/A_v^{q+}(E_i)\ .$$

The result of such an experiment is shown for S^{5+} in Fig. 2, where we have plotted these two ratios versus E_r. Several jumps appear in the data which are far beyond the range of statistical error. These jumps probably occur because of slit-edge scattering, which may vary somewhat with ion-beam steering at different energies. (Note that in our configuration the ion beam may be scattered at the narrow entrance aperture in the cathode.)

IV. DATA ANALYSIS

The ratio R_0 is composed of signal R_s plus background $R_b(V_y=0)$, whereas each R_v contains only background. Figure 3 is a plot of the difference (R_0-R_v) versus E_r and it can be seen that the "jumps" have disappeared. The jumps can be thought of as sudden changes in β in Eq. (4), but since they affect R_0 and R_v in the same way, subtraction of the two causes cancellation. It can be seen in Fig. 3 that above $E_r\simeq 17$ eV, even though R_s should equal zero, the measured difference is nonzero. This effect is due to pressure modulation caused by the electron-energy modulation. Looking again at the composition of R_0 and R_v,

$$R_0=R_s+\alpha P(V_y=0)E_i^{-n}+\beta E_i^{-m}\ ,$$

$$R_v=\alpha P(V_y=V_t)E_i^{-n}+\beta E_i^{-m}\ ,$$

we see that the difference

$$R_0-R_v=R_s+\alpha(\Delta P)E_i^{-n}\ ,$$

where

$$\Delta P=P(V_y=0)-P(V_y=V_t)\ .$$

We now choose a constant K such that the difference is zero where we expect no signal, i.e.,

$$R_s=(R_0-R_v)-KE_i^{-n}\ ,$$

where n is determined from R_v, and subtract this term from the difference in the region $0\leq E_r\lesssim E_m$ to yield R_s. This term (KE_i^{-n}) is shown as the solid curve in Fig. 3 and its typical magnitude is 5% of R_v.

The signal ratio R_s is related to the DR cross section σ by

$$R_s=\int\int \rho_i v_r\sigma(v_r)\rho_e(v_r)dv_r d\Omega \Big/ \int \rho_i v_i dA\ ,$$

where ρ_e is the electron density, ρ_i is the ion density, v_r is the relative velocity, v_i is the velocity of the ions, and Ω and A are the volume and cross-sectional area of the interaction region, a cylinder whose radius is that of the ion beam r_i and having the length of the electron beam L; since ρ_i and v_i are constant within Ω, the ion current

$$I_i=\int \rho_i v_i dA=\rho_i v_i A\ .$$

Approximating $\rho_e(v_r)$ by an average electron density $\bar{\rho}_e$, times a distribution in relative velocities $f(v_r)$, both being independent of position within Ω, we can write that

$$R_s=(\bar{\rho}_e L/v_i)\int v_r\sigma(v_r)f(v_r)dv_r$$
$$=(\bar{\rho}_e L/v_i)\langle v_r\sigma\rangle\ .$$

Thus, from the measured quantities, we can calculate $\langle v_r\sigma\rangle$ at every ion energy or relative energy, i.e., $\langle v_r\sigma\rangle=R_s v_i/\bar{\rho}_e L$.

V. COMPARISON OF THEORY AND EXPERIMENT

In order to compare our results to calculations, we shall first review the properties of the DR cross section σ and

then discuss how our particular experiment affects the theoretical predictions. The σ exhibits many sharp resonances (having widths $\ll 10^{-2}$ Ry), but for convenience of presentation and comparison with experiment it is useful to define $\bar{\sigma}$, averaged over an arbitrarily chosen energy interval Δe, as

$$\bar{\sigma}(E_r)=\frac{1}{\Delta e}\int_{E_r-\Delta e/2}^{E_r+\Delta e/2}\sigma\, de\ .$$

For $\Delta e=0.01$ Ry, which is much smaller than our experimental energy resolution, $\bar{\sigma}$ carries essentially the same information as σ itself. The σ predicted to be observed under the conditions of this experiment depends on the electric fields present in two regions; first, the charge-analysis region and second, the interaction region.

The electric field used for charge analysis can field-ionize states of the $A^{(q-1)+}(\alpha;n,l)$ having high n values. The maximum n state that can survive these fields is approximately given by[9]

$$n_m^4\simeq 6.31\times 10^8 q^3/E(\mathrm{V/cm})\ , \tag{5}$$

where q is the core charge and E is the analysis field in V/cm. In this experiment the deflection field used was $\sim$4 kV/cm, and for P^{4+}, S^{5+}, and Cl^{6+}, $n_m\simeq 60$, 65, and 76, respectively.

Less well understood is the effect of small fields in the interaction region[10] which can mix l states for a given n, and thereby increase the DR cross section. This increase can be easily understood from the following considerations. The dielectronic recombination cross section

$$\sigma_{\mathrm{DR}}\propto\sigma^{**}\left[\frac{A_r}{A_a+A_r}\right],$$

where σ^{**} is the cross section for formation of the doubly excited state of Eq. (1), A_r is the radiative rate leading to stabilization of this state, and A_a is the autoionizing rate. But since $\sigma^{**}\propto A_a$,

$$\sigma_{\mathrm{DR}}\propto A_r A_a/(A_r+A_a)\ , \tag{6}$$

and hence large σ_{DR} is expected for $A_a\gg A_r$, where $\sigma_{\mathrm{DR}}\propto A_r$.

With this in mind consider the l dependence of A_a for a given n: An example, $Mg^+ n=20$, is shown[10] in Fig. 4. The radiative rate A_r for the $\beta\rightarrow\alpha$ core relaxation is essentially independent of l, but A_a falls rapidly with l. If we make the assumption that all states with $A_a>A_r$ contribute to σ_{DR} and all states with $A_a<A_r$ do not, we find a total of 72 states which contribute. If we place the ion into a field strong enough to mix all the l states, we must now use the Stark representation[10] shown in Fig. 5. Using the same criteria as for Fig. 4, we find that 304 states should lead to DR; a gain in σ_{DR} of a factor of $\sim$4.2. Exact calculations as a function of applied field are still not available, but an approximation which assumes complete Stark mixing might be a useful upper limit for purposes of comparison of theory with experiment. Such calculations for our cases have been carried

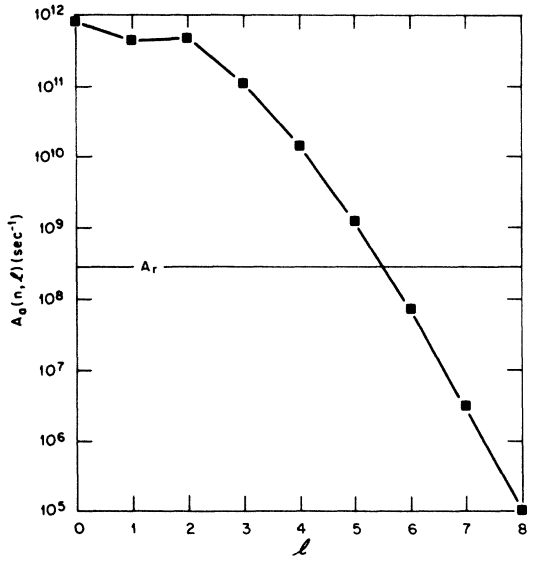

FIG. 4. $A_a(n,l)$ and A_r vs l in spherical coordinates for $n=20$ in Na-like Mg^+ from Ref. 10.

out for all n values less than $n_{\max}$, as calculated from Eq. (5), by Griffin, Pindzola, and Bottcher.[10] An example of this effect is shown in Fig. 6, where we show two histograms of $v_r\bar{\sigma}$ versus E_r for S^{5+} with $\Delta e=0.01$ Ry. The upper histogram assumes complete Stark mixing, the lower no mixing. If our experimental energy resolution were of the order of 0.1 eV, then our measured $\langle v_r\sigma\rangle$ versus E_r would look much like Fig. 6.

Even a cursory examination of Fig. 3 reveals a rather broad and asymmetric shape for the measured $\langle v_r\sigma\rangle$ rather than the predicted sharp peak of Fig. 6. If we assume that the energy dependence of $\bar{\sigma}$ is correctly calcu-

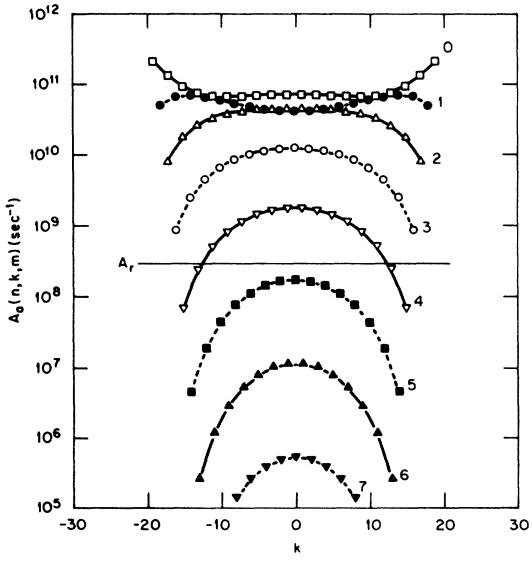

FIG. 5. $A_a(n,k,m)$ and A_r vs k in parabolic coordinates for $n=20$ in Na-like Mg^+ from Ref. 10. The number to the right of each curve drawn through the points equals $|m|$.

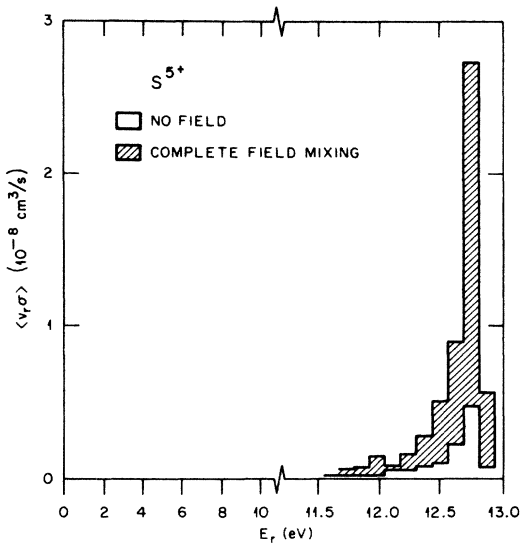

FIG. 6. DR rate $v_r\bar{\sigma}$ vs E_r for S^{5+} with $\Delta e=0.01$ Ry calculated from the $\bar{\sigma}$ of Ref. 10. Lower histogram without field mixing, upper histogram with complete mixing.

lated, it is almost a δ function on the scale of Fig. 3 and hence the measured shape of $\langle v_r\sigma\rangle$ is a reflection of the relative velocity distribution $f(v_r)$ present in our experiment.

Since the ions pass through an energy-analyzing magnet, a bending magnet, and several small apertures, their velocity is very well defined. Thus, we shall neglect the contribution of the narrow spread in ion velocities to $f(v_r)$ and consider only the contribution of the electron velocity distribution $f(v_e)$ to $f(v_r)$. The resulting $\langle v\sigma\rangle$ versus E_r [as defined in Eq. (3)] is affected differently by the component of $f(v_e)$ parallel to the ion beam, $f_{||}$, and by the transverse component, $f_\perp$. The signal from any resonance (or a 0.01-Ry energy bin) is distributed to higher and lower E_r by $f_{||}$, but only to lower E_r by $f_\perp$. Furthermore, the "width" of the energy spread due to $f_{||}$ varies as a function of E_r due to the center-of-mass while the effect of $f_\perp$ is constant with E_r. In an attempt to find an empirical velocity distribution to fit the data, we assumed the form of the two components of $f(v_e)$ to be

$$f_{||}=(\alpha/\sqrt{\pi})\exp[-\alpha^2(v_{||}-v_{||0})^2]$$

and

$$f_\perp=2\beta v_\perp\exp(-\beta^2 v_\perp^2)\,,$$

where $v_{||}$ and $v_\perp$ are the electron velocity components parallel and transverse to the ion beam, respectively, $v_{||_0}$ is the electron velocity determined by V_c, and α and β are constants. Here, $f_\perp$ is a two-dimensional Maxwellian distribution with a "temperature" determined by the cathode temperature, a compression factor[7] and other electron-flow factors, and $f_{||}$ is an "offset" (by $v_{||_0}$ from 0) one-dimensional Maxwellian distribution. Transformation to the center of mass leaves $f_\perp$ unchanged while $f_{||}$ becomes

$$f'_{||}=(\alpha/\sqrt{\pi})\exp[-\alpha^2(v'_{||}-v_0)^2]\,,$$

where the primes denote center of mass and v_0 is given by

$$v_0=(2E_r/m_e)^{1/2}\,.$$

Since we have no independent way of measuring the electron velocity distribution, we determined the constants α and β from our data. The calculated rate for Cl^{6+} was convoluted with $f'_{||}$ and $f_\perp$ and the constants varied until the shape of the resultant rate versus E_r agreed with the Cl^{6+} data. The values obtained by this fitting procedure were $\beta=7.55\times10^{-9}$ sec/cm and $\alpha=6.89\times10^{-8}$ sec/cm. These same values were then used to convolute the calculated rates for P^{4+} and S^{5+} and were found to be in reasonable agreement with the shape of the P^{4+} and S^{5+} data (as well as for other ions not reported here).

The results of this folding of the calculated rates and our data are shown in Figs. 7, 8, and 9 for P^{4+}, S^{5+}, and Cl^{6+}, respectively. The upper-solid line in each figure is the calculated rate for complete field mixing and the lower-solid curve corresponds to no mixing. The error bars on the data points are the relative uncertainties which include counting statistics and background subtraction for any one ion or between any two ions. The absolute uncertainty is dominated by the imprecise knowledge of the electron density, $\bar{\rho}_e$. Although beam profiles were measured by the manufacturer and ourselves, the measurements were made at only a few points in the six-dimensional continuum of cathode voltage, grid voltage, solenoidal field, and space. We estimate the uncertainty in $\bar{\rho}_e$ to be $\pm30\%$, and thus the absolute uncertainty of the data is approximately $\pm35\%$.

Due to the broad energy spread of our electron beam, no information regarding individual resonances can be deduced. Our rate measurements for all three ions fall between the calculations assuming no l mixing and complete

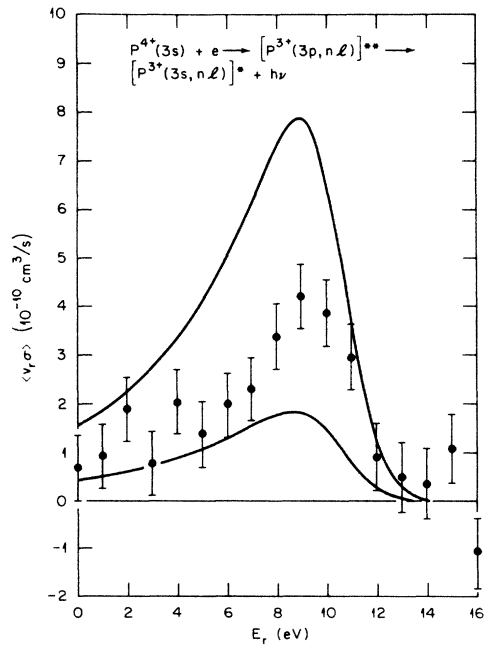

FIG. 7. DR rate $v_r\bar{\sigma}$ vs E_r for P^{4+}. Points are the experimental data, the upper curve is calculated from the $\bar{\sigma}$ of Ref. 10 with complete mixing and the lower curve is the same without field.

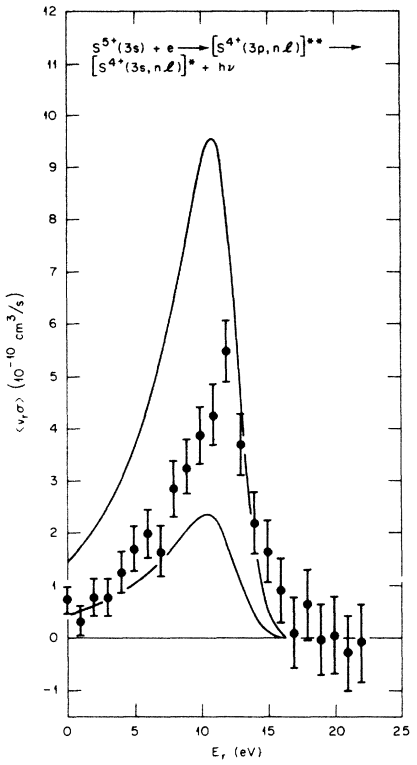

FIG. 8. DR rate $v_R\bar{\sigma}$ vs E_r for S^{5+}. Points are the experimental data, the upper curve is calculated from the $\bar{\sigma}$ of Ref. 10 with complete mixing, and the lower curve is the same without field.

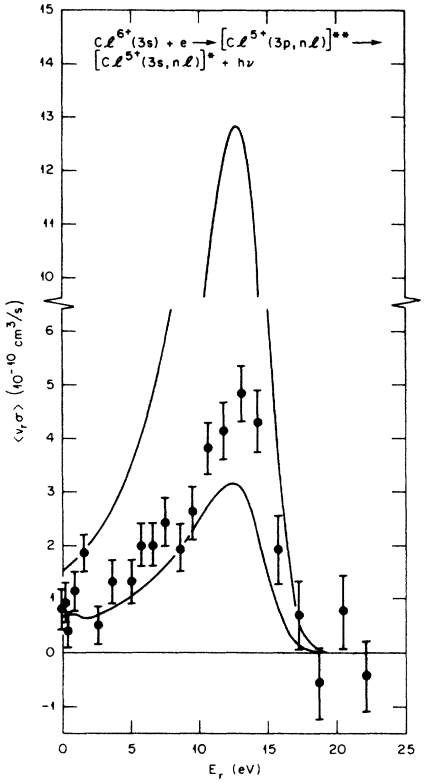

FIG. 9. DR rate $v_r\bar{\sigma}$ vs E_r for Cl^{6+}. Points are the experimental data, the upper curve is calculated from the $\bar{\sigma}$ of Ref. 10 with complete mixing and the lower curve is the same without field.

l mixing. The calculated peak values for the rates increase with increasing q; assuming complete mixing, $\langle v_r\sigma \rangle_{\max}=7.9$, 9.5, and 12.8 (in units of 10^{-10} cm^3/sec) for P^{4+}, S^{5+}, and Cl^{6+}, respectively, and 1.6, 2.3, and 3.2 assuming no mixing. The measured peak values for the rates are approximately constant at 4–5. The implication here is that field mixing is incomplete and that it is less complete for higher charge. Although no direct calculations exist on the field-enhancement effect for the cases discussed in this paper, some general statements can be made based upon calculations for Mg^+ (Na-like) and Li-like B^{2+} and C^{3+} ions. First, field effects on $\sigma_{DR}(n)$ can be quite large and grow larger with increasing n. Second, it takes very little field to saturate the field effects,[11] especially for high values of n (e.g., $\sim$80% saturation for a field of 10 V/cm for $n=30$ in B^{2+} and C^{3+}). Finally, the field effects on $\sigma_{DR}(n)$ should decrease for higher q values for a given n. The actual field present in the recombination region of our experiment is difficult to assess since it varies over the radius of the electron beam ranging from 0 V/cm at the center to 150 V/cm at the outer edge. Under ideal conditions the ion beam is confined to a region ± 0.25 mm from the electron-beam center, where the field reaches a value of only ~ 5 V/cm, but fields in the order ~ 10 V/cm are certainly imaginable. Similar comments can be made regarding the comparison of theory[10] with experiment for Mg^+, i.e., similar fields (24 V/cm) give similar results $\sigma_{\text{expt}}=1.1\times 10^{-17}$ cm^2, σ_{theor} (no mixing)$=0.2\times 10^{-17}$ cm^2, σ_{theor} (with complete mixing) $=1.7\times 10^{-17}$ cm^2.

A possible further cause for disagreement between our measured DR rates and those calculated from theory is that the $3p_{3/2}\rightarrow 3p_{1/2}$ autoionization channel was neglected[12] in the σ calculations. The energy differences between the $3p_{3/2}$ and $3p_{1/2}$ states for P^{4+}, S^{5+}, and Cl^{6+} are 98, 157, and 235 meV, respectively, so that Rydberg states having $n \gtrsim 46$ may autoionize. This causes an increase in A_a in the denominator in Eq. (6) but not in the numerator, and thus σ decreases. Since the field effects cause more enhancement of the DR rate for high-n states and since the $3p_{3/2}\rightarrow 3p_{1/2}$ autoionization causes dimunition of the DR rate for high-n states, the effect on the total DR rate will be a small decrease.

ACKNOWLEDGMENTS

We thank Dr. C. Bottcher, Dr. D. C. Griffin, Dr. Y. Hahn, Dr. K. LaGattuta, and Dr. M. S. Pindzola for many fruitful discussions concerning DR theory. We also thank J. M. Loftus and W. H. Hamley for their many years of apparatus construction and advice. One of us (C.M.F.) thanks the Oak Ridge Associated Universities for support under Travel Grant No. S-3039. This research was sponsored by the U.S. Department of Energy (Division of Basic Energy Sciences) under Contract No. DE-AC05-84OR21400 with Martin Marietta Energy Systems, Inc.

[1]M. Bitter *et al.*, Phys. Rev. Lett. **43**, 129 (1979).
[2]D. S. Belić, G. H. Dunn, T. J. Morgan, D. W. Mueller, and C. Timmer, Phys. Rev. Lett. **50**, 339 (1983).
[3]J. F. Williams, Phys. Rev. A **29**, 2936 (1984).
[4]J. B. A. Mitchell, C. T. Ng, J. L. Forand, D. P. Levac, R. E. Mitchell, A. Sen, D. B. Miko, and J. W. McGowan, Phys. Rev. Lett. **50**, 335 (1983).
[5]P. F. Dittner, S. Datz, P. D. Miller, C. D. Moak, P. H. Stelson, C. Bottcher, W. B. Dress, G. D. Alton, N. Nešković, and C. M. Fou, Phys. Rev. Lett. **51**, 31 (1983).
[6]Model 202-Ag-1, Hughes Aircraft Co., Electronic Dynamics Division, Torrance, CA.
[7]P. T. Kirstein, G. S. Kino, and W. E. Waters, *Space Charge Flow* (McGraw-Hill, New York, 1965), p. 153.
[8]A. S. Gilmour, Jr., Research Report No. EE495 (School of Electrical Engineering, Cornell University, Ithaca, NY), RADC-TN-61-188, 1961 (unpublished).
[9]H. A. Bethe and E. E. Salpeter, *Quantum Mechanics of One- and Two- Electron Atoms* (Springer, Berlin, 1957), p. 238.
[10]D. C. Griffin, M. S. Pindzola, and C. Bottcher, Oak Ridge National Laboratory Report No. ORNL/TM-9478, 1985 (unpublished).
[11]K. LaGattuta (private communication).
[12]D. Griffin (private communication).